SCIENCE CHINA
Information Sciences

• RESEARCH PAPER •

March 2025, Vol. 68, Iss. 3, 132206:1–132206:16
https://doi.org/10.1007/s11432-024-4148-7

Event-triggered leader-follower bipartite consensus control for nonlinear multi-agent systems under DoS attacks

Wei SU[1], Chaoxu MU[1*], Song ZHU[2], Ben NIU[3] & Changyin SUN[4]

[1]*School of Control Science and Engineering, Tianjin University, Tianjin 300072, China*
[2]*School of Mathematics, China University of Mining and Technology, Xuzhou 221116, China*
[3]*School of Control Science and Engineering, Dalian University of Technology, Dalian 116024, China*
[4]*School of Automation, Southeast University, Nanjing 210096, China*

Received 22 February 2024/Revised 21 May 2024/Accepted 5 September 2024/Published online 8 February 2025

Abstract Aiming at the consensus control problem of nonlinear multi-agent systems (MASs) under directed topology, a leader-follower bipartite consensus control strategy is proposed. This strategy takes into account the potential for denial-of-service (DoS) attacks and completely unknown system dynamics. Specifically, the bipartite consensus dynamics describes the cooperation and competition relationship between followers and the leader, that is, the follower chooses to move in accordance with or opposite to the leader according to its trajectory. In order to optimize the communication bandwidth and mitigate the impact of DoS attacks, the proposed consensus control scheme integrates the DoS attack detection mechanism and event-triggered mechanism. In addition, neural networks (NNs) are used to solve the nonlinear problem, and a speed function is designed to achieve the desired tracking performance, ensuring that all agents' tracking errors converge to a predefined set in a finite time. With the help of backstepping, graph theory, and Lyapunov stability theory, sufficient conditions for achieving bipartite consensus without Zeno behavior are established. Finally, the accuracy and feasibility of the theoretical analysis are verified by simulation cases.

Keywords multi-agent systems, neural networks, bipartite consensus, event-trigger, denial-of-service attack

Citation Su W, Mu C X, Zhu S, et al. Event-triggered leader-follower bipartite consensus control for nonlinear multi-agent systems under DoS attacks. Sci China Inf Sci, 2025, 68(3): 132206, https://doi.org/10.1007/s11432-024-4148-7

1 Introduction

In recent times, multi-agent systems (MASs) have found broad application across numerous domains, including sensor networks, formation control, and information fusion. The study of MASs has attracted considerable attention from researchers in various fields. The issue of consensus is a critical and fundamental concern in the realm of research on controlling distributed networks with MASs. Consensus refers to making the agents agree on some key quantities based on the designed appropriate distributed control protocol. Consensus can be divided into two categories (namely, leaderless consensus and leader-following consensus) based on the different roles that agents play in the system. So far, scholars have conducted extensive research on consensus control for MASs [1–4]. The development of sensor technology and computer technology has led to the emergence of several consensus subtopics with both practical and theoretical significance. These subtopics primarily include network topology consensus, communication delay consensus, finite time consensus, and more, as seen in [5–8]. However, the research results obtained in all the above literature are based on cooperative consensus control rather than bipartite consensus control. As a result, in the complex scenarios of practical applications, there are still many essential difficulties for the bipartite consensus problem of the nonlinear MASs. Further investigation and exploration are necessary.

Furthermore, it should be noted that each individual agent has been equipped with electronic technology devices, including embedded microprocessors and actuation modules, which enhance the agent's intelligence and capabilities. However, this also presents significant challenges in terms of limited communication bandwidth and energy supply for each agent. Motivated by the need for practical operational processes, researchers have conducted relevant studies on event-triggered control, as documented

* Corresponding author (email: cxmu@tju.edu)

in [9–14]. For instance, Ref. [11] introduced a method for event-triggered control based on relative information, aiming to mitigate the control effects of infinite fast execution in MASs. In [14], the research further considered the unpredictable traffic issue and designed the memory event-triggered scheme. Although some meaningful results on the event-triggered consensus control for nonlinear MASs have been published, the bound of the tracking error cannot be predefined in advance. Nevertheless, the problem of the tracking error converging to a predefined bound for nonlinear MASs under denial-of-service (DoS) attacks has not received the attention it deserves. Only a small amount of work has considered this issue, which motivated our research.

Meanwhile, note that a secure and reliable communication environment is an important prerequisite for the distributed consensus control of MASs. However, network attacks on MASs are becoming increasingly prevalent in open network environments, such as DoS attacks, deception attacks, and replay attacks, and their potential security threats from malicious attacks can have a devastating impact on the physical world. Especially to deserve mention, the communication topology is most vulnerable between agents due to some unavoidable DoS attacks in the various communication channels. Effective intelligent defense strategies have gained extensive attention from an increasing number of researchers, leading to many inspiring achievements (for instance [15–19], and the references cited therein). In [18], an event-triggered fault-tolerant control scheme based on local communication to mitigate the adverse effects of aperiodic DoS attacks for nonlinear MASs is proposed. Ref. [19] developed a low-pass filter distributed control protocol for the nonlinear MASs subjected to DoS attacks to achieve cooperative control. The above studies address the problem of DoS attacks blocking communication channels between agents. However, there are still few results on DoS attacks blocking information transmission channels between MAS components. This makes the controller design procedure very difficult and challenging, and greatly motivates our research interests.

Inspired by the above analysis, this article mainly develops an event-triggered communication strategy to solve the DoS attacks on the information transmission channels problem for leader-following nonlinear MASs, which can achieve MASs bipartite consensus tracking control with prescribed performance. The main contributions are summarized as follows. (i) Refs. [20–22] mainly focused on the general consensus problem of nonlinear MASs, while this paper is dedicated to the more specific issue of the bipartite consensus control problem. This is more extensive in the application scenario, offering greater practicality and significance, and meets the limitations of the traditional method in the specific environment. Through in-depth research and discussion of this problem, this paper puts forward a more accurate and feasible solution strategy. (ii) Compared with the traditional method [23–25], the proposed method optimizes the convergence rate and time of the system by designing a speed function in advance. This innovative design strategy ensures that all error orders converge the specified set within a predefined time frame, thus significantly improving the real-time performance and robustness of the control system. (iii) Refs. [26–28] mainly relied on residual differences between observations and system states to detect DoS attacks. However, when the communication channel between the observer and the controller is attacked, the detection mechanism will completely lose its effectiveness. To solve this problem, this paper proposes a DoS attack detection mechanism based on the logical relationship of voltage level signals from the outputs of the detection component. This novel detection method not only improves the accuracy of detection, but also remains effective when the communication channel is attacked, thus significantly enhancing the security and robustness of the system. (iv) Compared with the sample-based control method in [29, 30], this paper introduces an event-triggered communication strategy for nonlinear MASs which is more vulnerable to DoS attacks. This strategy aims to optimize system performance by reducing the update frequency of the controller, making the control input more resilient to the duration of DoS attacks. This strategy not only helps to reduce the computational burden, but also improves the system's anti-interference ability of the system in the presence of disturbances.

2 Problem preliminaries

2.1 System model

Consider the nonlinear MAS model based on a leader and N followers, where the followers' model structure is

$$\dot{x}_{i,a} = x_{i,a+1} + g_{i,a}\left(\bar{x}_{i,a}\right),$$

$$\begin{aligned} \dot{x}_{i,n} &= u_i + g_{i,n}\left(\bar{x}_{i,n}\right), \\ y_i &= x_{i,1}, \end{aligned} \tag{1}$$

where $i = 1, 2, \ldots, N$, $a = 1, 2, \ldots, n-1$, and the notations $x_{i,a}$, u_i, and y_i are used to represent the system state, input, and output variables. Moreover, note that $\bar{x}_{i,a} = [x_{i,1}, x_{i,2}, \ldots, x_{i,a}] \in \mathbb{R}^a$ and $g_{i,a}$ is a nonlinear smooth function.

Assumption 1 ([31]). The leader's dynamic is represented by $y_d(t)$, and its first and second derivatives are characterized by being continuous and bounded, namely $\dot{y}_d$ and $\ddot{y}_d$.

Control goal: based on the graph theory, the speed function, the DoS attack detection mechanism, and the controller update rules, this paper aims to construct a distributed controller for the MASs model (1). This controller is designed to achieve bipartite consensus with predefined performance, even when the considered MASs are under DoS attacks.

Lemma 1 ([32]). For each O and Δ satisfying $\Delta \in \mathbb{R}$ and $O > 0$, the following inequality is true:

$$0 \leqslant |\Delta| - \Delta \tanh\left(\frac{\Delta}{O}\right) \leqslant 0.2785O. \tag{2}$$

Lemma 2 ([33]). For any given real number z and positive number k_Θ with $|z| < k_\Theta$, the inequality

$$\log \frac{k_\Theta^{2\Phi}}{k_\Theta^{2\Phi} - z^{2\Phi}} \leqslant \frac{z^{2\Phi}}{k_\Theta^{2\Phi} - z^{2\Phi}} \tag{3}$$

holds, where Φ is a positive constant.

2.2 Graph theory

The $\mathcal{G} = \left(\bar{\mathcal{V}}, \bar{\mathcal{E}}, \bar{\mathcal{A}}\right)$ refers to a digraph that serves as a model for communication among N agents. The set of nodes is defined as $\bar{\mathcal{V}} = (v_1, v_2, \ldots, v_N)$, and the set of edges is $\bar{\mathcal{E}} \subseteq \bar{\mathcal{V}} \times \bar{\mathcal{V}}$. Additionally, an adjacency matrix $\bar{\mathcal{A}} = [a_{ij}] \in \mathbb{R}^{N \times N}$ is defined, along with an in-degree matrix $\bar{\mathcal{D}} = \operatorname{diag}[d_1, d_2, \ldots, d_N]$ and a Laplacian matrix $\bar{\mathcal{L}}$. The relationship between matrices $\bar{\mathcal{A}}, \bar{\mathcal{D}}, \bar{\mathcal{L}}$ is expressed as $\bar{\mathcal{L}} = \bar{\mathcal{D}} - \bar{\mathcal{A}}$. This equation provides a clear understanding of their interconnectivity. Point out that a_{ij} indicates whether node i can get information from node j; if $a_{ij} > 0$, it can be obtained; otherwise $a_{ij} = 0$, moreover, $d_i = \sum_{j=1}^{N} a_{ij}$. Next, a directed graph $\bar{\mathcal{G}}$ is further introduced which is made up of graph $\mathcal{G}$, the leader, and the edges connecting the leader and followers. We use the notation $\bar{\mathcal{B}} = \operatorname{diag}[b_1, b_2, \ldots, b_N]$ to describe direct information transmission between the leader and the followers. Here, $b_i > 0$ means that the follower can communicate directly with the leader. Conversely, if $b_i = 0$, it indicates otherwise. Additionally, we use $\bar{\mathcal{H}}$ to represent the graph matrix, and define $\bar{\mathcal{H}} = \bar{\mathcal{L}} + \bar{\mathcal{B}}$.

Assumption 2 ([34]). There is a spanning tree in $\bar{\mathcal{G}}$ where the root node is the leader.

2.3 Speed function

This paper introduces a class of rate functions defined as

$$\bar{v}(t) = \begin{cases} \left(\frac{\bar{\mathcal{T}}}{\bar{\mathcal{T}} - t}\right)^4 v(t), & 0 < t < \bar{\mathcal{T}}, \\ \infty, & t > \bar{\mathcal{T}}, \end{cases} \tag{4}$$

where $v(t)$ represents a set of smooth functions that satisfy the constraints $v(0) = 1$ and $\dot{v}(t) \geqslant 0$. The parameter $\bar{\mathcal{T}}$ represents a finite time that can be determined by the designer. Additionally, to ensure continuity of $\bar{v}(t)$ everywhere, we define $\lim_{t \to \bar{\mathcal{T}}^-} (\frac{\bar{\mathcal{T}}}{\bar{\mathcal{T}} - t})^4 v(t) = \infty$.

In accordance with (4), we can derive the mathematical expression of the speed function as

$$\beta(t) = \frac{1}{(1 - a^*)\,\bar{v}(t)^{-1} + a^*} \tag{5}$$

with a^* as a parameter satisfying $0 < a^* \ll 1$; furthermore, we can rewrite the speed function using (4) and (5) as follows:

$$\beta(t) = \begin{cases} \frac{\bar{\mathcal{T}}^4 v(t)}{(1-a^*)\left(\bar{\mathcal{T}}-t\right)^4 + a^* \bar{\mathcal{T}}^4 v(t)}, & 0 \leqslant t < \bar{\mathcal{T}}, \\ \frac{1}{a^*}, & t > \bar{\mathcal{T}}. \end{cases} \tag{6}$$

Assumption 3 ([35]). A designed time in the condition $\bar{\mathcal{T}}$ meets $\bar{\mathcal{T}} > \bar{\mathcal{T}}_c$, where $\bar{\mathcal{T}}_c$ represents a small time interval for signal transmission and processing.

2.4 Neural networks approximation

NNs have the ability to deal with uncertain or unknown systems. This paper introduces the radial basis function (RBF) NNs $\theta^{*\mathrm{T}}\Delta\left(\bar{\mathcal{Z}}\right)$ to approximate unknown smooth nonlinear function

$$\Psi\left(\bar{\mathcal{Z}}\right) = \theta^{*\mathrm{T}}\Delta\left(\bar{\mathcal{Z}}\right) + \tau\left(\bar{\mathcal{Z}}\right) \tag{7}$$

over a compact set $\Omega_{\bar{\mathcal{Z}}} \subset \mathbb{R}^q$. The approximation error $\tau\left(\bar{\mathcal{Z}}\right)$ satisfies $|\tau\left(\bar{\mathcal{Z}}\right)| \leqslant \varepsilon$, and ε is a desired error. The weight vector $\theta = [\theta_1, \ldots, \theta_N]^{\mathrm{T}}$, the basis function vector $\Delta(\bar{\mathcal{Z}}) = [\Delta_1(\bar{\mathcal{Z}}), \ldots, \Delta_N\left(\bar{\mathcal{Z}}\right)]^{\mathrm{T}}$, the RBF NN nodes number $N > 1$. Define the ideal constant weight vector θ^* as

$$\theta^* = \arg\min_{\theta \in \mathbb{R}^N} \left\{ \sup_{\bar{\mathcal{Z}} \in \Omega_{\bar{\mathcal{Z}}}} \left| \Psi\left(\bar{\mathcal{Z}}\right) - \theta^{\mathrm{T}}\Delta\left(\bar{\mathcal{Z}}\right) \right| \right\}, \tag{8}$$

and Gaussian function $\Delta_i\left(\bar{\mathcal{Z}}\right)$ is selected as

$$\Delta_i\left(\bar{\mathcal{Z}}\right) = \exp\left[-\frac{\left(\bar{\mathcal{Z}} - \mu_i\right)^{\mathrm{T}}\left(\bar{\mathcal{Z}} - \mu_i\right)}{\eta_i^2} \right], i = 1, 2, \ldots, N, \tag{9}$$

where $\mu_i = [\mu_{i1}, \mu_{i2}, \ldots, \mu_{iN}]^{\mathrm{T}}$ is the center of the receptive field and η_i is the width of the $\Delta_i\left(\bar{\mathcal{Z}}\right)$.

2.5 Valid and invalid DoS attacks

The objective of DoS attacks is to hinder the communication channel of the event-triggered components and render the consensus control and energy-saving strategy ineffective. To be more precise, we categorize DoS attacks as either valid or invalid.

For agent i, the sequence of valid DoS attacks is defined as $\left\{\bar{h}_l^i\right\}_{l \in N_D}$, where $\bar{h}_l^i \geqslant 0$ and N_D represents the total number of DoS attacks. The time interval of the lth valid attack is defined as $\bar{\mathcal{H}}_i = \left\{\bar{h}_l^i\right\} \cup \left[\bar{h}_l^i, \bar{h}_l^i + \bar{o}_l^i\right)$, and $\bar{o}_l^i \in \mathbb{R}^+$ represents the length of the valid one. One point worth noting is that this paper considers at least one successful control input attempt to update during the time interval of the valid DoS attack.

Then, for any interval $[t_1, t_2]$, let

$$\bar{\mathcal{D}}_i(t_1, t_2) = \cup_{l \in N_D}\left[\bar{h}_l^i, \bar{h}_l^i + \bar{o}_l^i\right) \cap [t_1, t_2], \tag{10}$$

$$\bar{\mathcal{H}}_i(t_1, t_2) = \cup_{l \in N_D}\left[\bar{h}_l^i + \bar{o}_l^i, \bar{h}_{l+1}^i\right) \cap [t_1, t_2], \tag{11}$$

where $\bar{\mathcal{D}}_i(t_1, t_2)$ and $\bar{\mathcal{H}}_i(t_1, t_2)$ are the union of valid and invalid DoS attacks.

Further, we can get

$$\bar{\mathcal{H}}_i(t_1, t_2) = [t_1, t_2] \setminus \bar{\mathcal{D}}_i(t_1, t_2), \tag{12}$$

$$\left|\bar{\mathcal{H}}_i(t_1, t_2)\right| = t_2 - \left|\bar{\mathcal{D}}_i(t_1, t_2)\right|. \tag{13}$$

Assumption 4 ([27]). There is $T > 1$ and $\varsigma \in \mathbb{R}^+$, so that $|\mathcal{D}(t_1, t_2)| \leqslant \varsigma + ([t_2 - t_1]/T)$ is true, for any $0 \leqslant t_1 < t_2$.

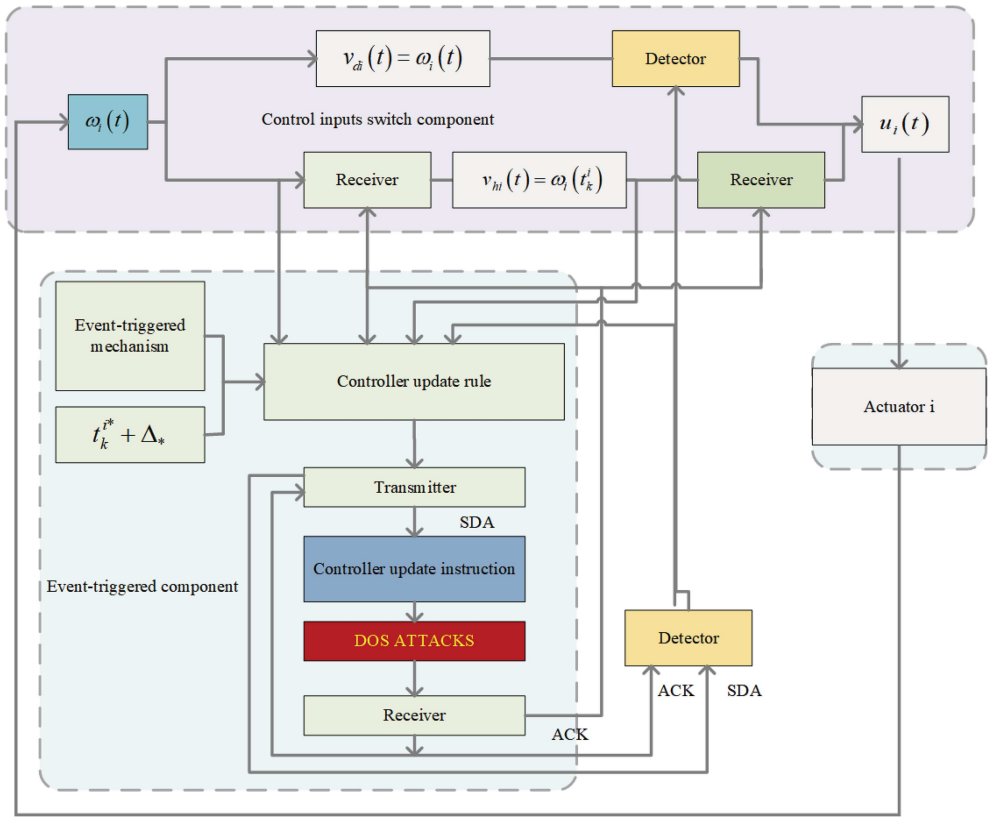

Figure 1 (Color online) Framework of DoS attacks detection mechanism.

3 Control strategy

This part illustrates the detection mechanism for DoS attacks, controller switching, and update rules to facilitate the design of the bipartite consensus control algorithm.

3.1 DoS attacks detection mechanism

Note that $u_i(t)=\iota_i v_{hi}(t)+(1-\iota_i)v_{di}(t)$, ι_i is the controller switch signal, and $v_{hi}(t)$ and $v_{di}(t)$ are the controller in safe status and DoS attacks status. A detector has been designed to identify the occurrence of DoS attacks, as illustrated in Figure 1. The transmitter and receiver components of the detector generate two outputs, namely SDA and ACK. These outputs are represented by high (1) and low (0) voltage levels. It is important to note that, initially, the SDA signal is set to the high level (1) and the ACK signal is set to the low level (0). The detection mechanism comprises two parts. The first part utilizes event-triggered communication (15) to detect when the systems are in a safe state. The second part utilizes resilient periodic control to detect when the systems are under a valid attack. At the update instant t_{r+1}^*, the SDA signal transitions from high (1) to low (0). In the event of invalid DoS attacks, the receiver can retrieve the low level voltage of SDA, triggering the ACK signal to change from low (0) to high (1), which then activates event-triggered communication to update the control input vhi. Once these operations have been completed, the SDA and ACK return to their original high and low voltages. If the receiver component is unable to obtain the low SDA signal, it indicates that the system has been subjected to valid DoS attacks. In such a scenario, the periodic update policy (14) is activated, and an attempt is made to update the control input v_{di} at regular intervals of Δ_*.

Based on the description above, the mechanism for detecting DoS attacks and the corresponding switching signal ι_i can be summarized as follows.

(1) When SDA = 1, ACK = 0, and $\iota_i = 1$, this indicates that the system control input signal is operating safely based on the signal updated at the last trigger moment $v_{hi}(t)=\omega_i(t_k^i)$ in (48).

(2) If SDA = 0, ACK = 0, and $\iota_i = 0$, it indicates that the channel between the transmitting and receiving components has been blocked by a DoS attack. This puts the system in a state of DoS attack

status, which triggers the activation of the periodic resilient mechanism. At each time step Δ_*, the control input attempts to update the value of $v_{di}(t) = \omega_i(t)$ in (65).

(3) When SDA = 0, ACK = 1, and $\iota_i = 1$, this means that the system is in a safe status, and the event-triggered mechanism (15) is activated to update the control input $v_{hi}(t) = \omega_i\left(t_{k+1}^i\right)$.

3.2 Controller updates rule

For any $k \in N$, the control signal update rule for v_{hi} is given as

$$t_{k+1}^{i*} = \begin{cases} t_k^{i*} + \Delta_*, & \text{if } k \in \mathcal{F}_i, \\ t_{r+1}^i, & \text{otherwise}, \end{cases} \tag{14}$$

where $\mathcal{F}_i = \left\{k \in N_0 | t_k^{i*} \in \cup_{l \in N_D} \bar{\mathcal{H}}_i\right\}$, Δ_* is a constant, and $\Delta_* > 0$.

When the channel is open between the transmitter and receiver components, event-triggered communication operates normally. The controller's v_{hi} update rules are as follows:

$$t_{r+1}^i = \inf\left\{t > t_r^i \left| |e_i(t)| \geqslant \bar{\rho}_{i1} |v_{hi}(t)| + \bar{\rho}_{i2}\right.\right\}, \tag{15}$$

where $0 < \bar{\rho}_{i1} < 1$ and $\bar{\rho}_{i2} > 0$ are positive design parameters, and event-triggered error $e_i(t)$ will be designed later.

4 Controller design

This part aims to develop a distributed controller that utilizes Lyapunov theory and backstepping technique to achieve bipartite consensus for MASs. However, since DoS attacks can occur randomly, we will be discussing two different scenarios: A when the system is in a safe state, and B when the system is under a valid attack.

4.1 Control design in safe status

We introduce the agent i synchronization error and the associated coordinate transformations as follows:

$$s_{i,1} = \sum_{j=1}^{N} |a_{ij}| \left(y_i - \text{sign}(a_{ij}) y_j\right) + |b_i| \left(y_i - \text{sign}(b_i) y_d\right), \ 1 \leqslant i \leqslant N, \tag{16}$$

$$s_{i,a} = x_{i,a} - \alpha_{i,a-1}, \ 2 \leqslant a \leqslant n, \tag{17}$$

$$z_{i,a} = \beta_i s_{i,a}, \ 1 \leqslant a \leqslant n, \tag{18}$$

where $\alpha_{i,a-1}$ is the virtual control input and β_i is described in (6). Since $\beta_i(0) = 1$, one gets $z_{i,a}(0) = s_{i,a}(0)$. b_i is the edge weight of the ith follower dynamic node to the virtual reference node y_d in the network topology.

Step 1: By taking the derivative of (16) and combining it with the studied system model (1), we can obtain

$$\dot{s}_{i,1} = h_i \left(x_{i,2} + g_{i,1}\right) - \sum_{j=1}^{N} a_{ij} \left(x_{j,2} + g_{j,1}\right) - b_i \dot{y}_d, \tag{19}$$

where $h_i = |b_i| + d_i$.

Following the formula (18), the following equation holds:

$$\dot{z}_{i,1} = \beta_i \left(R_i s_{i,1} + h_i \left(g_{i,1} + x_{i,2}\right) - \sum_{j=1}^{N} a_{ij} \left(g_{j,1} + x_{j,2}\right) - b_i \dot{y}_d\right), \tag{20}$$

where $R_i = \beta_i^{-1} \dot{\beta}_i$.

To attain the desired level of performance as prescribed, the barrier Lyapunov function is established as

$$V_{i,1}=\frac{1}{4}\log\frac{k_{i,1}^4}{k_{i,1}^4-z_{i,1}^4}+\frac{1}{2\rho_{i,1}}\tilde{W}_{i,1}^2+\frac{1}{2r_{i,1}}\tilde{\pi}_{i,1}^2, \tag{21}$$

where $|z_{i,1}|<k_{i,1}$, $k_{i,1}>0$, $\rho_{i,1}>0$, $r_{i,1}>0$ are design parameters, and define $\tilde{W}_{i,1}=W_{i,1}^*-\hat{W}_{i,1}$ and $\tilde{\pi}_{i,1}=\pi_{i,1}^*-\hat{\pi}_{i,1}$. Here, $\hat{W}_{i,1}$ and $\hat{\pi}_{i,1}$ are the estimation of $W_{i,1}^*$ and $\pi_{i,1}^*$, respectively.

Upon calculation of the derivative of $V_{i,1}$, the resulting equation is as follows:

$$\begin{aligned}\dot{V}_{i,1}=&\frac{z_{i,1}^3\beta_i}{k_{i,1}^4-z_{i,1}^4}\left(h_i\left(s_{i,2}+\alpha_{i,1}\right)+R_is_{i,1}+h_ig_{i,1}-\sum_{j=1}^{N}a_{ij}\left(x_{j,2}+g_{j,1}\right)-b_i\dot{y}_d\right)\\&-\frac{1}{\rho_{i,1}}\tilde{W}_{i,1}\dot{\hat{W}}_{i,1}-\frac{1}{r_{i,1}}\tilde{\pi}_{i,1}\dot{\hat{\pi}}_{i,1}.\end{aligned} \tag{22}$$

Construct the following unknown nonlinear function $\Psi_{i,1}$. Because $\Psi_{i,1}$ cannot be directly used for developing the controller, by utilizing RBF NNs (7) to estimate it, one can obtain

$$\begin{aligned}\Psi_{i,1}\left(\bar{\mathcal{Z}}_{i,1},\bar{\mathcal{Z}}_{j,1}\right)&=h_ig_{i,1}-\sum_{j=1}^{N}a_{ij}\left(x_{j,2}+g_{j,1}\right)-b_i\dot{y}_d\\&=\theta_{i,1}^{*\mathrm{T}}\Delta_{i,1}\left(\bar{\mathcal{Z}}_{i,1},\bar{\mathcal{Z}}_{j,1}\right)+\tau_{i,1}^*\left(\bar{\mathcal{Z}}_{i,1},\bar{\mathcal{Z}}_{j,1}\right),\end{aligned} \tag{23}$$

where $\bar{\mathcal{Z}}_{i,1}=[x_{i,1},y_d,\dot{y}_d]$, $\bar{\mathcal{Z}}_{j,1}=[x_{j,1},x_{j,2}]$. $\theta_{i,1}^*$ is the NN vector, $\Delta_{i,1}$ is the NN basis function, and the approximation error $\tau_{i,1}^*$ with $\left|\tau_{i,1}^*\right|<\varepsilon_{i,1}$, $\varepsilon_{i,1}>0$ is a unknown constant.

Applying Young's inequality, one has

$$\frac{z_{i,1}^3\beta_i\Psi_{i,1}}{k_{i,1}^4-z_{i,1}^4}\leqslant\frac{z_{i,1}^6\beta_i^2W_{i,1}^*\|\Delta_{i,1}\|^2}{2\bar{c}_{i,1}^2\left(k_{i,1}^4-z_{i,1}^4\right)^2}+\frac{\bar{c}_{i,1}^2}{2}+\frac{z_{i,1}^6\beta_i^2\varepsilon_{i,1}^2}{2\left(k_{i,1}^4-z_{i,1}^4\right)^2}+\frac{1}{2}, \tag{24}$$

$$\frac{h_iz_{i,1}^3z_{i,2}}{k_{i,1}^4-z_{i,1}^4}\leqslant\frac{3h_iz_{i,1}^4}{4\left(k_{i,1}^4-z_{i,1}^4\right)^{\frac{4}{3}}}+\frac{h_iz_{i,2}^4}{4}, \tag{25}$$

where $\bar{c}_{i,1}$ is a positive parameter, $W_{i,1}^*=\left\|\theta_{i,1}^*\right\|^2$, and $\pi_{i,1}=\varepsilon_{i,1}^2$.

Substituting (23)–(25) into (22), one gets

$$\begin{aligned}\dot{V}_{i,1}=&\frac{z_{i,1}^3\beta_i}{k_{i,1}^4-z_{i,1}^4}\left(R_is_{i,1}+h_i\alpha_{i,1}+\frac{z_{i,1}^3\beta_iW_{i,1}^*\|\Delta_{i,1}\|^2}{2\bar{c}_{i,1}^2\left(k_{i,1}^4-z_{i,1}^4\right)}+\frac{3h_is_{i,1}}{4\left(k_{i,1}^4-z_{i,1}^4\right)^{\frac{1}{3}}}\right)\\&+\frac{z_{i,1}^6\beta_i^2\pi_{i,1}}{2(k_{i,1}^4-z_{i,1}^4)^2}+\frac{h_iz_{i,2}^4}{4}+\frac{\bar{c}_{i,1}^2}{2}+2-\frac{1}{\rho_{i,1}}\tilde{W}_{i,1}\dot{\hat{W}}_{i,1}-\frac{1}{r_{i,1}}\tilde{\pi}_{i,1}\dot{\hat{\pi}}_{i,1}.\end{aligned} \tag{26}$$

Based on (26), it can be inferred that the virtual control signal and adaptive law are as follows:

$$\alpha_{i,1}=\frac{1}{h_i}\left(-R_is_{i,1}-P_{i,1}s_{i,1}-\frac{z_{i,1}^3\beta_i\hat{W}_{i,1}\|\Delta_{i,1}\|^2}{2\bar{c}_{i,1}^2\left(k_{i,1}^4-z_{i,1}^4\right)}-\frac{3h_is_{i,1}}{4\left(k_{i,1}^4-z_{i,1}^4\right)^{\frac{1}{3}}}-\frac{z_{i,1}^3\beta_i\hat{\pi}_{i,1}}{2\left(k_{i,1}^4-z_{i,1}^4\right)}\right), \tag{27}$$

$$\dot{\hat{W}}_{i,1}=\frac{\rho_{i,1}}{2\bar{c}_{i,1}^2}\frac{z_{i,1}^6\beta_i^2\|\Delta_{i,1}\|^2}{\left(k_{i,1}^4-z_{i,1}^4\right)^2}-\bar{\rho}_{i,1}\hat{W}_{i,1}, \tag{28}$$

$$\dot{\hat{\pi}}_{i,1}=\frac{r_{i,1}z_{i,1}^6\beta_i^2}{2\left(k_{i,1}^4-z_{i,1}^4\right)^2}-\bar{r}_{i,1}\hat{\pi}_{i,1}, \tag{29}$$

where $\bar{r}_{i,1}$, $\bar{\rho}_{i,1}$, and $P_{i,1}$ are the designed positive constants.

According to the definition of $\tilde{W}_{i,1}$ and $\tilde{\pi}_{i,1}$ in (21), we have

$$\tilde{W}_{i,1}W_{i,1}^{*} \leqslant \frac{1}{2}W_{i,1}^{*2} - \frac{1}{2}\tilde{W}_{i,1}^{2}, \tag{30}$$

$$\tilde{\pi}_{i,1}\dot{\hat{\pi}}_{i,1} \leqslant \frac{1}{2}\pi_{i,1}^{2} - \frac{1}{2}\tilde{\pi}_{i,1}^{2}. \tag{31}$$

Putting (27)–(31) into (26) produces

$$\dot{V}_{i,1} \leqslant -\frac{P_{i,1}z_{i,1}^{4}}{k_{i,1}^{4}-z_{i,1}^{4}} - \frac{\bar{\rho}_{i,1}}{2\rho_{i,1}}\tilde{W}_{i,1}^{2} - \frac{\bar{r}_{i,1}}{2r_{i,1}}\tilde{\pi}_{i,1}^{2} + \frac{h_i z_{i,2}^{4}}{4} + \Lambda_{i,1}, \tag{32}$$

where $\Lambda_{i,1} = \frac{\bar{\rho}_{i,1}}{2\rho_{i,1}}W_{i,1}^{*2} + \frac{\bar{c}_{i,1}^{2}}{2} + 2 + \frac{\bar{r}_{i,1}}{2r_{i,1}}\pi_{i,1}^{2}$.

Step a $(2 \leqslant a \leqslant n-1)$**:** Consider the following barrier Lyapunov function candidate $V_{i,a}$:

$$V_{i,a} = \frac{1}{4}\log\frac{k_{i,a}^{4}}{k_{i,a}^{4}-z_{i,a}^{4}} + \frac{1}{2\rho_{i,a}}\tilde{W}_{i,a}^{2} + \frac{1}{2r_{i,a}}\tilde{\pi}_{i,a}^{2}. \tag{33}$$

Differentiating (33) shows that

$$\dot{V}_{i,a} = \frac{z_{i,a}^{3}\beta_i}{k_{i,a}^{4}-z_{i,a}^{4}}\left(R_i s_{i,a} + x_{i,a+1} + g_{i,a} - \dot{\alpha}_{i,a-1}\right) - \frac{1}{\rho_{i,a}}\tilde{W}_{i,a}\dot{\hat{W}}_{i,a} - \frac{1}{r_{i,a}}\tilde{\pi}_{i,a}\dot{\hat{\pi}}_{i,a}, \tag{34}$$

where

$$\begin{aligned}\dot{\alpha}_{i,a-1} = {} & \frac{\partial\alpha_{i,a-1}}{\partial x_{i,a-1}}\left(x_{i,a}+g_{i,a-1}\right) + \sum_{q=1}^{k}\sum_{j=1}^{N}\frac{\partial\alpha_{i,a-1}}{\partial x_{j,q}}\left(x_{j,q+1}+g_{j,q}\right) + \sum_{q=1}^{k-1}\frac{\partial\alpha_{i,a-1}}{\partial\hat{W}_{i,q}}\dot{\hat{W}}_{i,q} \\ & + \sum_{q=1}^{k-1}\frac{\partial\alpha_{i,a-1}}{\partial\hat{\pi}_{i,q}}\dot{\hat{\pi}}_{i,q} + \sum_{q=0}^{k-1}\frac{\partial\alpha_{i,a-1}}{\partial y_d^{(q)}}y_d^{(q+1)} + \sum_{q=0}^{k-1}\frac{\partial\alpha_{i,a-1}}{\partial\beta_i^{(q)}}\beta_i^{(q+1)}.\end{aligned} \tag{35}$$

Construct the following unknown nonlinear function $F_{i,r}$:

$$\Psi_{i,a} = \left(\bar{\mathcal{Z}}_{i,a}, \bar{\mathcal{Z}}_{j,a}\right) = g_{i,a} - \dot{\alpha}_{i,a-1}, \tag{36}$$

where

$$\overline{\mathcal{Z}}_{i,a} = \left[[x_{i,1},\ldots,x_{i,k}]^{\mathrm{T}}, \left[\hat{W}_{i,1},\ldots,\hat{W}_{i,k-1}\right]^{\mathrm{T}}, \left[y_d,\dot{y}_d,\ldots,y_d^{(k)}\right]^{\mathrm{T}}, [\hat{\pi}_{i,1},\ldots,\hat{\pi}_{i,k-1}]^{\mathrm{T}}, \left[\beta_i,\dot{\beta}_i,\ldots,\beta_i^{(k)}\right]^{\mathrm{T}}\right], \tag{37}$$

$$\bar{\mathcal{Z}}_{j,a} = [x_{i,1},\ldots,x_{j,k+1}]^{\mathrm{T}}. \tag{38}$$

Similar to the procedure (23)–(25) in Step 1, the virtual controller $\alpha_{i,a}$ and the adaptation laws $\dot{\hat{W}}_{i,a}$ and $\dot{\hat{\pi}}_{i,a}$ are developed as

$$\alpha_{i,a} = -R_i s_{i,a} - P_{i,a}s_{i,a} - \frac{z_{i,a}^{3}\beta_i\hat{W}_{i,r}\|\Delta_{i,a}\|^{2}}{2\bar{c}_{i,a}^{2}\left(k_{i,a}^{4}-z_{i,a}^{4}\right)} - \frac{3s_{i,a}}{4\left(k_{i,a}^{4}-z_{i,a}^{4}\right)^{\frac{1}{3}}} - \frac{z_{i,a}^{3}\beta_i\hat{\pi}_{i,a}}{2\left(k_{i,a}^{4}-z_{i,a}^{4}\right)}, \tag{39}$$

$$\dot{\hat{W}}_{i,a} = \frac{\rho_{i,a}}{2\bar{c}_{i,a}^{2}}\frac{z_{i,a}^{6}\beta_i^{2}\|\Delta_{i,a}\|^{2}}{\left(k_{i,a}^{4}-z_{i,a}^{4}\right)^{2}} - \bar{\rho}_{i,a}\hat{W}_{i,a}, \tag{40}$$

$$\dot{\hat{\pi}}_{i,a} = \frac{r_{i,a}z_{i,a}^{6}\beta_i^{2}}{2\left(k_{i,a}^{4}-z_{i,a}^{4}\right)^{2}} - \bar{r}_{i,a}\hat{\pi}_{i,a}. \tag{41}$$

Moreover, Eq. (34) can be replaced by

$$\dot{V}_{i,a} \leqslant -\frac{P_{i,a}z_{i,a}^{4}}{k_{i,a}^{4}-z_{i,a}^{4}} - \frac{\bar{r}_{i,a}}{2r_{i,a}}\tilde{\pi}_{i,a}^{2} - \frac{\bar{\rho}_{i,a}}{2\rho_{i,a}}\tilde{W}_{i,a}^{2} + \frac{z_{i,a+1}^{4}}{4} + \Lambda_{i,a}, \tag{42}$$

where $\Lambda_{i,a}=\frac{\bar{\rho}_{i,a}}{2\rho_{i,a}}W_{i,a}^{*2}+\frac{\bar{r}_{i,a}}{2r_{i,a}}\pi_{i,a}^{2}+\frac{\bar{c}_{i,a}^{2}}{2}+\frac{1}{2}$.

Step n**:** According to (13), we know that

$$\dot{z}_{i,n}=\beta_i\left(R_i s_{i,n}+u_i+g_{i,n}-\dot{\alpha}_{i,n-1}\right). \tag{43}$$

The last step proposes the barrier Lyapunov function as a potential solution as follows:

$$V_{i,n}=\frac{1}{4}\log\frac{k_{i,n}^{4}}{k_{i,n}^{4}-z_{i,n}^{4}}+\frac{1}{2\rho_{i,n}}\tilde{W}_{i,n}^{2}+\frac{1}{2r_{i,n}}\tilde{\pi}_{i,n}^{2}. \tag{44}$$

Upon calculation of the derivative of $V_{i,n}$, the resulting equation is

$$\dot{V}_{i,n}=\frac{z_{i,n}^{3}\beta_i}{k_{i,n}^{4}-z_{i,n}^{4}}\left(R_i s_{i,n}+u_i-\dot{\alpha}_{i,n-1}+g_{i,n}\right)-\frac{1}{\rho_{i,n}}\tilde{W}_{i,n}\dot{\hat{W}}_{i,n}-\frac{1}{r_{i,n}}\tilde{\pi}_{i,n}\dot{\hat{\pi}}_{i,n}, \tag{45}$$

where $a=n$ and $\dot{\alpha}_{i,n-1}=\dot{\alpha}_{i,a-1}$.

Define the following unknown nonlinear functions $\Psi_{i,n}$:

$$\Psi_{i,n}\left(\bar{\mathcal{Z}}_{i,n},\bar{\mathcal{Z}}_{j,n}\right)=g_{i,n}-\dot{\alpha}_{i,n-1}=\theta_{i,n}^{*\mathrm{T}}\Delta_{i,n}\left(\bar{\mathcal{Z}}_{i,n},\bar{\mathcal{Z}}_{j,n}\right)+\varepsilon_{i,n}^{*}\left(\bar{\mathcal{Z}}_{i,n},\bar{\mathcal{Z}}_{j,n}\right), \tag{46}$$

where $\bar{\mathcal{Z}}_{i,n}=\bar{\mathcal{Z}}_{i,a}$, $\bar{\mathcal{Z}}_{j,n}=\bar{\mathcal{Z}}_{j,a}$, and $a=n$.

From (43)–(46), we have

$$\dot{V}_{i,n}=\frac{z_{i,n}^{3}\beta_i}{k_{i,n}^{4}-z_{i,n}^{4}}\left(R_i s_{i,n}+u_i+g_{i,n}\right)-\frac{1}{r_{i,n}}\tilde{\pi}_{i,n}\dot{\hat{\pi}}_{i,n}-\frac{1}{\rho_{i,n}}\tilde{W}_{i,n}\dot{\hat{W}}_{i,n}. \tag{47}$$

Next, we develop the controller v_{hi} as

$$v_{hi}(t)=w_i\left(t_k^{i}\right),\forall t\in\left[t_k^{i},t_{k+1}^{i}\right), \tag{48}$$

where $w_i(t)$ is a subsequently designed event-triggered control law.

According to $|e_i(t)|<\bar{\rho}_{i1}|v_{hi}|+\bar{\rho}_{i2}$, one obtains

$$\begin{cases} e_i(t)=\lambda_i(t)\left(\bar{\rho}_{i1}v_{hi}+\bar{\rho}_{i2}\right), v_{hi}\geqslant 0,\\ e_i(t)=\lambda_{i1}(t)\,\bar{\rho}_{i1}v_{hi}+\lambda_{i2}(t)\,\bar{\rho}_{i2}, v_{hi}<0, \end{cases} \tag{49}$$

where $0<\bar{\rho}_{i1}<1$, $0<\bar{\rho}_{i2}<1$, $\lambda_i\in[-1,1]$, and $\lambda_{i1}=-\lambda_{i2}$.

From (49), the following

$$e_i=\lambda_{i1}\bar{\rho}_{i1}v_{hi}+\lambda_{i2}\bar{\rho}_{i2} \tag{50}$$

is true with λ_{i1} and λ_{i2} satisfying

$$\begin{cases} \lambda_{i1}=-\lambda_{i2}, v_{hi}\geqslant 0,\\ \lambda_{i1}=\lambda_{i2}, v_{hi}<0. \end{cases} \tag{51}$$

Then, we obtain

$$v_{hi}(t)=\frac{w_i(t)}{1+\lambda_{i1}\bar{\rho}_{i1}}-\frac{\lambda_{i2}\bar{\rho}_{i2}}{1+\lambda_{i1}\bar{\rho}_{i1}}. \tag{52}$$

The controller is designed according to the event-triggered mechanism as

$$w_i(t)=-\frac{1+\bar{\rho}_{i1}}{1-\bar{\rho}_{i1}}\bar{\rho}_{i2}\alpha_{i,n}\tanh\left(\frac{z_{i,n}^{3}\beta_i\bar{\rho}_{i2}\alpha_{i,n}}{\left(k_{i,n}^{4}-z_{i,n}^{4}\right)(1-\bar{\rho}_{i1})\,\tau_i}\right), \tag{53}$$

where τ_i is design constants.

Substituting (48)–(53) into (47) yields

$$\dot{V}_{i,n}=\frac{z_{i,n}^3\beta_i}{k_{i,n}^4-z_{i,n}^4}\left(R_is_{i,n}+\frac{w_i\left(t\right)}{1+\lambda_{i1}\bar{\rho}_{i1}}-\frac{\lambda_{i2}\bar{\rho}_{i2}}{1+\lambda_{i1}\bar{\rho}_{i1}}+\Psi_{i,n}\right)-\frac{1}{r_{i,n}}\tilde{\pi}_{i,n}\dot{\hat{\pi}}_{i,n}-\frac{1}{\rho_{i,n}}\tilde{W}_{i,n}\dot{\hat{W}}_{i,n}. \tag{54}$$

Based on Lemma 1, one gets

$$\begin{aligned}\frac{z_{i,n}^3\beta_i}{k_{i,n}^4-z_{i,n}^4}\frac{w_i\left(t\right)}{1+\lambda_{i1}\bar{\rho}_{i1}}&\leqslant-\frac{z_{i,n}^3\beta_i}{k_{i,n}^4-z_{i,n}^4}\frac{\bar{\rho}_{i2}}{1-\bar{\rho}_{i1}}\tanh\left(\frac{z_{i,n}^3\beta_i\bar{\rho}_{i2}}{\left(k_{i,n}^4-z_{i,n}^4\right)\left(1-\bar{\rho}_{i1}\right)\tau_i}\right)\\&\leqslant-\frac{\left|z_{i,n}^3\beta_i\right|}{\left(k_{i,n}^4-z_{i,n}^4\right)\left(1-\bar{\rho}_{i1}\right)}+0.2785\tau_i,\end{aligned} \tag{55}$$

$$\begin{aligned}-\frac{z_{i,n}^3\beta_i}{k_{i,n}^4-z_{i,n}^4}\frac{\lambda_{i2}\bar{\rho}_{i2}}{1+\lambda_{i1}\bar{\rho}_{i1}}&\leqslant\frac{\left|z_{i,n}^3\beta_i\right|}{\left(k_{i,n}^4-z_{i,n}^4\right)}\left|\frac{\lambda_{i2}\bar{\rho}_{i2}}{1+\lambda_{i1}\bar{\rho}_{i1}}\right|\\&\leqslant\frac{\left|z_{i,n}^3\beta_i\right|\bar{\rho}_{i2}}{\left(k_{i,n}^4-z_{i,n}^4\right)\left(1-\bar{\rho}_{i1}\right)},\end{aligned} \tag{56}$$

where $1+\lambda_{i1}\bar{\rho}_{i1}\leqslant1+\bar{\rho}_{i1}$ and $|\frac{\lambda_{i2}\bar{\rho}_{i2}}{1+\lambda_{i1}\bar{\rho}_{i1}}|\leqslant\frac{\bar{\rho}_{i2}}{1-\bar{\rho}_{i1}}$.

The computation of (54) is got as

$$\begin{aligned}\dot{V}_{i,n}=&\frac{z_{i,n}^3\beta_i}{k_{i,n}^4-z_{i,n}^4}\left(R_is_{i,n}+\alpha_{i,n}+\frac{z_{i,n}^3\beta_iW_{i,n}^*\|\Delta_{i,n}\|^2}{2\bar{c}_{i,n}^2\left(k_{i,n}^4-z_{i,n}^4\right)}+\frac{s_{i,n}\left(k_{i,n}^4-z_{i,n}^4\right)}{4}\right)\\&-\frac{z_{i,n}^4}{4}+\frac{\bar{c}_{i,n}^2}{2}-\frac{1}{r_{i,n}}\tilde{\pi}_{i,n}\dot{\hat{\pi}}_{i,n}+\frac{1}{2}+0.2785\tau_i+\frac{z_{i,n}^6\beta_i^2\pi_{i,n}}{2\left(k_{i,n}^4-z_{i,n}^4\right)^2}-\frac{1}{\rho_{i,n}}\tilde{W}_{i,n}\dot{\hat{W}}_{i,n}.\end{aligned} \tag{57}$$

The adaptive laws and the controller are constructed as

$$\alpha_{i,n}=-P_{i,n}s_{i,n}-R_is_{i,n}-\frac{z_{i,n}^3\beta_i\hat{W}_{i,n}\|\Delta_{i,n}\|^2}{2\bar{c}_{i,n}^2\left(k_{i,n}^4-z_{i,n}^4\right)}-\frac{s_{i,n}\left(k_{i,n}^4-z_{i,n}^4\right)}{4}-\frac{z_{i,n}^3\beta_i\hat{\pi}_{i,n}}{2\left(k_{i,n}^4-z_{i,n}^4\right)}, \tag{58}$$

$$\dot{\hat{W}}_{i,n}=\frac{\rho_{i,n}}{2\bar{c}_{i,n}^2}\frac{z_{i,n}^6\beta_i^2\|\Delta_{i,n}\|^2}{\left(k_{i,n}^4-z_{i,n}^4\right)^2}-\bar{\rho}_{i,n}\hat{W}_{i,n}, \tag{59}$$

$$\dot{\hat{\pi}}_{i,n}=\frac{r_{i,n}z_{i,n}^6\beta_i^2}{2\left(k_{i,n}^4-z_{i,n}^4\right)^2}-\bar{r}_{i,n}\hat{\pi}_{i,n}. \tag{60}$$

Combining (57)–(60) produces

$$\dot{V}_{i,n}\leqslant-\frac{P_{i,n}z_{i,n}^4}{k_{i,n}^4-z_{i,n}^4}-\frac{\bar{\rho}_{i,n}}{2\rho_{i,n}}\tilde{W}_{i,n}^2-\frac{\bar{r}_{i,n}}{2r_{i,n}}\tilde{\pi}_{i,n}^2-\frac{z_{i,n}^4}{4}+\Lambda_{i,n}, \tag{61}$$

where $\Lambda_{i,n}=\frac{\bar{\rho}_{i,n}}{2\rho_{i,n}}W_{i,n}^{*2}+\frac{\bar{r}_{i,n}}{2r_{i,n}}\pi_{i,n}^2+\frac{\bar{c}_{i,n}^2}{2}+\frac{1}{2}+0.2785\tau_i$.

We choose the following total Lyapunov functions:

$$V_i=\sum_{a=1}^{n}V_{i,a}. \tag{62}$$

Then, we can get

$$\dot{V}_i\leqslant-\sum_{a=1}^{n}\left(-\frac{P_{i,a}z_{i,a}^4}{k_{i,a}^4-z_{i,a}^4}-\frac{\bar{\rho}_{i,a}}{2\rho_{i,a}}\tilde{W}_{i,a}^2-\frac{\bar{r}_{i,a}}{2r_{i,a}}\tilde{\pi}_{i,a}^2+\Lambda_{i,a}\right). \tag{63}$$

Next, we have

$$V=\sum_{i=1}^{n}V_i\leqslant-c_oV+c_1, \tag{64}$$

where $c_o=\min\left\{2P_{i,a},\bar{\rho}_{i,a},\bar{r}_{i,a}\right\}$ and $c_1=\sum_{i=1}^{n}\sum_{a=1}^{n}\Lambda_{i,a}$.

4.2 Control design in valid DoS attacks

When the event-triggered component is subjected to an attack, the controller $v_{di}(t)$ is activated.

Let

$$v_{di}(t) = \omega_i(t), \tag{65}$$

where $\omega_i(t)$ is developed as shown in (53) with $\bar{\rho}_{i1} = 0$. Furthermore, we use the same process (48)–(61) for designing the controller and adaptive laws but with different control parameters, resulting in

$$\alpha_{i,n}^D = -P_{i,n}^D s_{i,n} - R_i^D s_{i,n} - \frac{z_{i,n}^3 \beta_i \hat{W}_{i,n} \|\Delta_{i,n}\|^2}{2\bar{c}_{i,n}^{D^2}\left(k_{i,n}^4 - z_{i,n}^4\right)} - \frac{s_{i,n}\left(k_{i,n}^4 - z_{i,n}^4\right)}{4} - \frac{z_{i,n}^3 \beta_i \hat{\pi}_{i,n}}{2\left(k_{i,n}^4 - z_{i,n}^4\right)}, \tag{66}$$

$$\dot{\hat{W}}_{i,n} = \frac{\rho_{i,n}^D}{2\bar{c}_{i,n}^{D^2}} \frac{z_{i,n}^6 \beta_i^2 \|\Delta_{i,n}\|^2}{\left(k_{i,n}^4 - z_{i,n}^4\right)^2} - \bar{\rho}_{i,n}^D \hat{W}_{i,n}, \tag{67}$$

$$\dot{\hat{\pi}}_{i,n} = \frac{r_{i,n}^D z_{i,n}^6 \beta_i^2}{2\left(k_{i,n}^4 - z_{i,n}^4\right)^2} - \bar{r}_{i,n}^D \hat{\pi}_{i,n}. \tag{68}$$

Then, we have

$$\dot{V}_n \leqslant -c_0^D V + c_1^D, \tag{69}$$

where $c_0^D = \min\left\{2P_{i,a}^D, \bar{\rho}_{i,a}^D, \bar{r}_{i,a}^D\right\}$ and $c_1^D = \sum_{i=1}^n \sum_{a=1}^n \Lambda_{i,a}^D = \sum_{i=1}^n \sum_{a=1}^n (\frac{\bar{\rho}_{i,a}^D}{2\rho_{i,a}^D} W_{i,n}^{*^2} + \frac{\bar{r}_{i,a}^D}{2r_{i,a}^D} \pi_{i,n}^{*^2} + \frac{\bar{c}_{i,a}^{D^2}}{2} + \frac{1}{2} + 0.2785\tau_i)$.

The proof process and adaptive laws are designed for case A and the same as those for case B. Therefore, the process for case B can refer to the previous proof process for case A.

4.3 Stability analysis

The results of case A and case B are summarized as follows:

$$\begin{cases} \dot{V}_n \leqslant -c_0 V_n + c_1 \leqslant -c_0 V_n + c^*, \text{ invalid attacks}, \\ \dot{V}_n \leqslant -c_2 V_n + c_3 \leqslant -c_2 V_n + c^*, \text{ valid attacks}, \end{cases} \tag{70}$$

where $c^* = \max\{c_1, c_2\}$.

From (64) and (69), when $t_a \in \left(\bar{h}_\iota + o_\iota, \bar{h}_{\iota+1}\right)$, the event-triggered component is not attacked, one gets

$$V_n(t_a) \leqslant \mathrm{e}^{-c_0\left(t_a - \left(\bar{h}_\iota + o_\iota\right)\right)} V_n\left(\bar{h}_\iota + o_\iota\right) + \frac{c^*}{c_0}. \tag{71}$$

When $t_b \in \left(\bar{h}_{\iota+1}, \bar{h}_{\iota+1} + o_{\iota+1}\right)$, the event-triggered component is attacked, one obtains

$$V_n(t_b) \leqslant \mathrm{e}^{-c_2\left(t_a - \left(\bar{h}_{\iota+1}\right)\right)} V_n\left(\bar{h}_{\iota+1}\right) + \frac{c^*}{c_2}. \tag{72}$$

Based on (71) and (72), we analyze the MASs (1) stability as the two cases.

Case A: $t \in \left(\bar{h}_\kappa + o_\kappa, \bar{h}_{\kappa+1}\right)$,

$$V_n(t) \leqslant \mathrm{e}^{-c_2 \bar{\mathcal{D}}_{(\kappa)}} \mathrm{e}^{-c_0 \bar{\mathcal{H}}_{(\kappa)}} \mathrm{e}^{-c_0\left(t - \left(\bar{h}_\kappa + o_\kappa\right)\right)} V_n(0) + \frac{c^*}{\sigma}, \tag{73}$$

where $c = \min\{c_0, c_2\}$, and the lengths of the disjoint unions of $\bar{\mathcal{D}}_\iota$ and $\bar{\mathcal{H}}_\iota$, where $\iota = 1, 2, \ldots, \kappa$, are defined as $\bar{\mathcal{D}}_{(\kappa)}$ and $\bar{\mathcal{H}}_{(\kappa)}$.

Since $\bar{\mathcal{H}}(0,t) = t - \bar{\mathcal{D}}(0,t)$, the following equality holds:

$$\mathrm{e}^{-c_2 \bar{\mathcal{D}}_{(\kappa)}} \mathrm{e}^{-c_0 \bar{\mathcal{H}}_{(\kappa)}} = \mathrm{e}^{-(c_2 - c_0)\bar{\mathcal{D}}_{(\kappa)}} \mathrm{e}^{-c_0 t}. \tag{74}$$

Then, we know

$$V_n(t) \leqslant \xi_{\mathcal{H}} \mathrm{e}^{-c_0 t} V_n(0) + \frac{c^*}{c}, \tag{75}$$

where $\xi_{\mathcal{H}} = \mathrm{e}^{-(c_2-c_0)\bar{\mathcal{D}}_{(\kappa)}}$.

Case B: $t \in \left(\bar{h}_{\kappa+1}, \bar{h}_{\kappa+1} + o_{\kappa+1}\right)$,

$$V_n(t) \leqslant \mathrm{e}^{-c_2\bar{\mathcal{D}}_{(\kappa)}} \mathrm{e}^{-c_0\bar{\mathcal{H}}_{(\kappa+1)}} \mathrm{e}^{-c_2\left(t-\left(\bar{h}_{\kappa+1}\right)\right)} V_n(0) + \frac{c^*}{\sigma}. \tag{76}$$

According to (70), we obtain

$$\mathrm{e}^{-c_2\bar{\mathcal{D}}_{(\kappa)}} \mathrm{e}^{-c_0\bar{\mathcal{H}}_{(\kappa+1)}} = \mathrm{e}^{-(c_2-c_0)\left(\varsigma+\frac{t}{T}\right)} \mathrm{e}^{-c_0 t}. \tag{77}$$

From the above analysis, we have

$$V_n(t) \leqslant \xi_{\mathcal{D}} \mathrm{e}^{-\left(c_0+c_2+\frac{c_2-c_0}{T}\right)t} V_n(0) + \frac{c^*}{c}, \tag{78}$$

where $\xi_{\mathcal{D}} = \mathrm{e}^{-(c_2-c_0)\varsigma} \mathrm{e}^{c_2\bar{h}_{o+1}}$.

Based on (61), (69), (75), (78), it can be inferred that $\xi_{\mathcal{H}}$, $\xi_{\mathcal{D}}$, c_0, and c_2 are all positive constants. We will now analyze two cases to further understand the behavior of the system. In case A, as time $t \to \infty$, the term $\mathrm{e}^{-c_0 t} \to 0$ and $V_n(t) \to \frac{c^*}{c}$. Next, based on (78), we will analyze case B: since the fact that $\frac{1}{T} < 1$, we can see that $\mathrm{e}^{-\left(c_0+c_2+\frac{c_2-c_0}{T}\right)t} \to 0$ as $t \to \infty$, and $V_n(t) \to \frac{c^*}{c}$ remains bounded. By referencing (44), (58)–(60), we can determine that z_{il}, $\hat{\theta}_i$, and $\hat{\theta}_{ij}$ for $i, j = 1, 2, \ldots, N$, $l = 1, 2, \ldots, n$ are all bounded. From (64) and (16), we can deduce that the values of $y_i - y_d$ and $y_i + y_d$ are bounded for $i = 1, 2, \ldots, N$. This implies that the output of all the followers can achieve bipartite consensus with the desired trajectory of the leader. Additionally, by utilizing (27) and (32), along with the bounded parameters of z_{i1}, $\hat{\theta}_i$, $\hat{\theta}_{ij}$, Δ_{i1}, and Δ_{j1}, we can further conclude that x_{i2} is also bounded. Then, it is noted that α_{i1} remains bounded. Next, by following a similar procedure, we can establish the boundedness of α_{iq} and $x_{i,q+1}$ for $q = 2, 3, \ldots, n-1$. By examining (64) and (69), it is evident that $u_i(t)$ is also bounded. Therefore, the boundedness of all signals in the closed-loop systems is guaranteed.

4.4 Without Zeno behavior

First, we make the assumption that the triggered interval, T_i, is equal to the difference between the times l and $l+1$, defined as $T_i = t_{l+1}^i - t_l^i$. Our objective is to prove $T_i > t_l^*$, where t_l^* is a positive value. To do this, we can use the fact that $e_i(t) = \omega_i(t) - u_i(t)$, $\forall t \in \left[t_l^i, t_{l+1}^i\right)$; one obtains

$$\frac{\mathrm{d}}{\mathrm{d}t}|e_i(t)| = \frac{\mathrm{d}}{\mathrm{d}t}(e_i(t) \times e_i(t))^{\frac{1}{2}} = \operatorname{sign}(e_i(t))\dot{e}_i(t) \leqslant |\dot{\omega}_i(t)|. \tag{79}$$

From this, we can deduce that $\omega_i(t)$ is a differentiable function and that $\dot{\omega}_i(t)$ includes all the bounded signals. This means that there exists a constant ς such that $|\dot{\omega}_i(t)| < \varsigma$. By using this information, we can demonstrate that $t_l^* \geqslant \left(\left[e_i(t) - e_i\left(t_l^i\right)\right]/\varsigma\right) \geqslant \left(\left[\bar{\rho}_{i1}|u_{i1}(t)| + \bar{\rho}_{i2}\right]/\varsigma\right) \geqslant (\bar{\rho}_{i2}/\varsigma) > 0$. By setting t_l^* in this way, the Zeno behavior is excluded.

5 Simulation study

To further verify that the designed controller can achieve the bipartite tracking control results with predefined performance. The communication topology of the MASs is described in Figure 2, where the follower is labeled 1, 2, 3, 4, 5 and the leader is labeled 0. The five followers is structurally balanced with $\mathcal{V}_1 = \{2, 4, 5\}$ and $\mathcal{V}_2 = \{1, 3\}$. It is pointed out that the relationship between agents in $\mathcal{V}_1$ and $\mathcal{V}_2$ is cooperation, while the relationship between $\mathcal{V}_1$ and $\mathcal{V}_2$ is competition. The considered multiple single-link robot systems (Figure 3) are modeled as follows:

$$M_i\ddot{Q}_i + \frac{1}{2}m_i^* G L_i \sin(Q_i) = \tau_i^*,$$

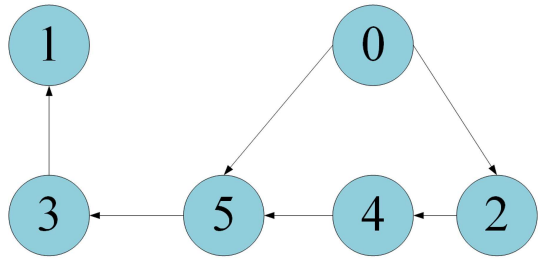

Figure 2 (Color online) Framework of the signal-link robot of one agent.

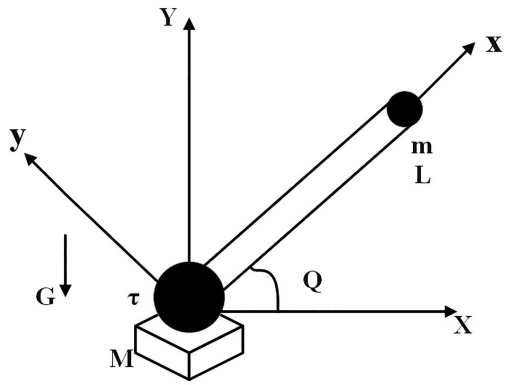

Figure 3 (Color online) Communication topology of MASs (1).

$$y_i = Q_i, \tag{80}$$

where $i = 1, 2, \ldots, 5$, the rotor inertia $M_i = 1$ kg, and the gravitational acceleration $G = 9.8$ m/s^2. Q_i denotes the angle position, $\dot{Q}_i$ represents the angle velocity of the link, and $\ddot{Q}_i$ is the angle acceleration. The mass of the link $m_i^* = 0.3$ kg and the length of the link $L_i = 0.3$ m. τ_i^* stands for the link's control force.

By defining $x_{i,1} = Q_i$ and $x_{i,2} = Q_i$, the systems (80) can be further expressed as

$$\begin{aligned} \dot{x}_{i,1} &= x_{i,2}, \\ \dot{x}_{i,2} &= u_i + g_{i,2}\left(\bar{x}_{i,2}\right), \\ y_i &= \dot{x}_{i,1}, \end{aligned} \tag{81}$$

where $g_{i,2}\left(\bar{x}_{i,2}\right) = -\frac{1}{2} m_i^* G L_i \sin\left(x_{i,1}\right)$ and the leader's signal $y_d\left(t\right) = \sin\left(6t\right)$. To accomplish this, we set the finite time $\bar{\mathcal{T}} = 2$ s and $b_i^* = 0.05$. Additionally, we choose $k_{i,a} = 1.5$ such that the predefined region $\Omega_{i,a} := \{s_{i,a} : |s_{i,a}| \leqslant 0.06\}$, where $a = 1, 2$. To begin the simulation, the initial values for the system are set as $\left[x_{1,1}\left(0\right), x_{1,2}\left(0\right)\right] = [-0.5, -0.35]$, $\left[x_{2,1}\left(0\right), x_{2,2}\left(0\right)\right] = [0.6, 0.2]$, $\left[x_{3,1}\left(0\right), x_{3,2}\left(0\right)\right] = [0.35, 0.4]$, $\left[x_{4,1}\left(0\right), x_{4,2}\left(0\right)\right] = [0.4, 0.3]$, and $\left[x_{5,1}\left(0\right), x_{5,2}\left(0\right)\right] = [-0.4, -0.1]$. The designed parameters are given as $\rho_i = 0.5$, $\sigma_i = 0.4$, $\tau_i = 1$, $p_1 = 15$, $p_2 = 55$, $\rho_{i,1} = 1$, $\bar{\rho}_{i,1} = 70$, $\rho_{i,2} = 0.7$, $\bar{\rho}_{i,2} = 80$, $\bar{\varsigma}_{i,2} = 120$, $\iota_i = 90$, and $\bar{\iota}_i = 200$. The control protocol is carried out based on the MATLAB platform, and the experimental simulation results in Figures 4–9 are obtained. Specifically, Figure 4 clearly displays the position and velocity trajectories of each agent. Notably, followers 1, 3, and 5 exhibit consistent position and velocity with the leader, while followers 2 and 4 demonstrate opposing position and velocity. Additionally, Figure 7 depicts the dynamic response of each follower at the event-triggered moment, with the ordinate representing the ith follower. It can be seen from Figure 7 that the event-triggered moment is different for different agents, avoiding Zeno behavior. Figure 8 demonstrates the superior performance of the proposed method in performing typical trajectories such as horizontal, vertical, and circular motions.

6 Conclusion

We have implemented bipartite tracking control for uncertain nonlinear MASs under DoS attack with predefined performance. A reliable mechanism for detecting DoS attacks is established based on the logical relationship between the signal output voltage level of physical components. At the same time, the communication bandwidth and energy resources can be saved by applying an event-triggered mechanism. This paper introduces RBF NNs to estimate completely unknown nonlinear functions. By designing barrier Lyapunov functions and speed functions that align with the characteristics of the system model, a novel control protocol is developed for designing a distributed controller. This algorithm has been verified to successfully realize bipartite tracking control, ensuring that all errors converge to a specified set within a given time. Additionally, all signals remain bounded, and Zeno behavior can be avoided. Finally, simulation results provide confirmation of the accuracy of the presented theoretical methodology. Future

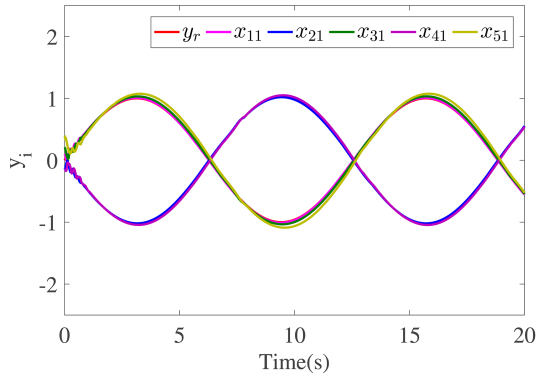

Figure 4 (Color online) Tracking performance of followers and leader.

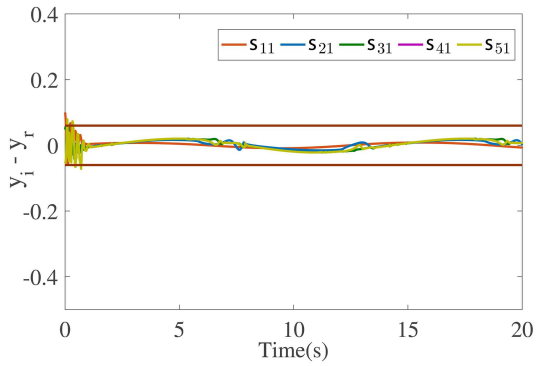

Figure 5 (Color online) All agents' synchronization errors.

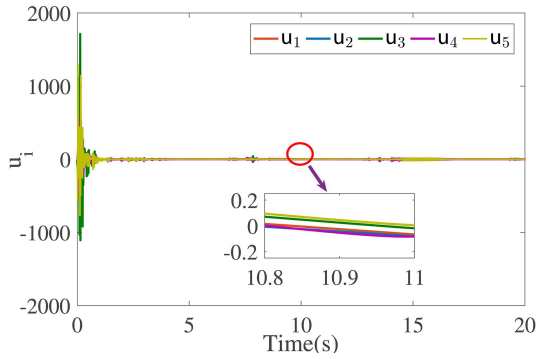

Figure 6 (Color online) All agents' control input signals.

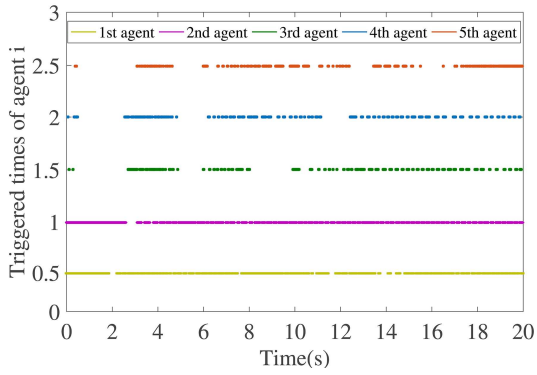

Figure 7 (Color online) Triggered release instants of all input signals.

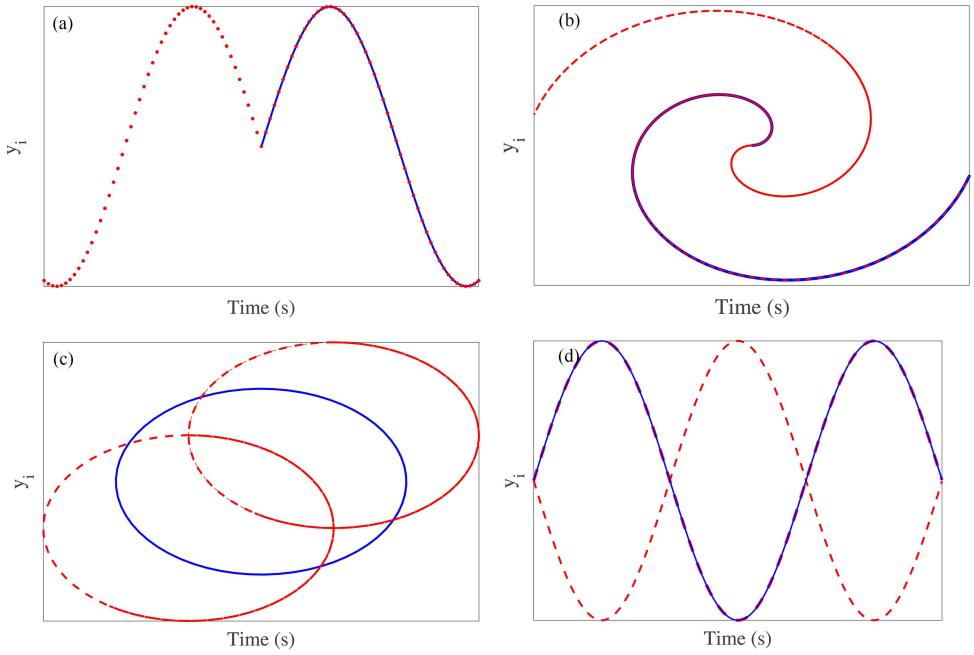

Figure 8 (Color online) Followers track the leader's different movement trajectories. (a) Sine wave; (b) logarithmic spiral; (c) ellipse; (d) cosine wave.

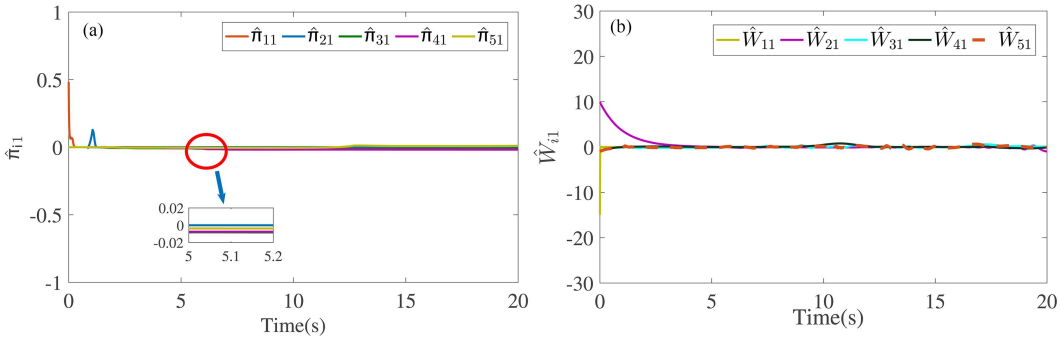

Figure 9 (Color online) Trajectories of adaptive laws (a) $\hat{\pi}_{i1}$ and (b) $\hat{W}_{i1}$.

work will be dedicated to further optimizing the DoS attack detection method based on multi-sensor fusion, and investigating the design of intelligent switching logic to select the most appropriate detection strategy in various scenarios.

Acknowledgements This work was supported by National Key Research and Development Program of China (Grant No. 2021YFB1714700) and National Natural Science Foundation of China (Grant No. 62333016).

References

1 Ding L, Han Q L, Guo G. Network-based leader-following consensus for distributed multi-agent systems. Automatica, 2013, 49: 2281–2286
2 Mu C, Peng J. Learning-based cooperative multiagent formation control with collision avoidance. IEEE Trans Syst Man Cybern Syst, 2022, 52: 7341–7352
3 Brittain M, Wei P. Scalable autonomous separation assurance with heterogeneous multi-agent reinforcement learning. IEEE Trans Automat Sci Eng, 2022, 19: 2837–2848
4 Mu C, Zhao Q, Sun C. Optimal model-free output synchronization of heterogeneous multiagent systems under switching topologies. IEEE Trans Ind Electron, 2019, 67: 10951–10964
5 Hu W, Cheng Y, Yang C. Leader-following consensus of linear multi-agent systems via reset control: a time-varying systems approach. Automatica, 2023, 149: 110824
6 Jiang J, Jiang Y. Leader-following consensus of linear time-varying multi-agent systems under fixed and switching topologies. Automatica, 2020, 113: 108804
7 Zhao G, Hua C. Leader-following consensus of multiagent systems via asynchronous sampled-data control: a hybrid system approach. IEEE Trans Automat Contr, 2021, 67: 2568–2575
8 Yang Y, Si X, Yue D, et al. Time-varying formation tracking with prescribed performance for uncertain nonaffine nonlinear multiagent systems. IEEE Trans Automat Sci Eng, 2020, 18: 1778–1789
9 Yan B, Shi P, Lim C C. Robust formation control for nonlinear heterogeneous multiagent systems based on adaptive event-triggered strategy. IEEE Trans Automat Sci Eng, 2021, 19: 2788–2800
10 Shahvali M, Naghibi-Sistani M B, Askari J. Distributed adaptive dynamic event-based consensus control for nonlinear uncertain multi-agent systems. Proc Inst Mech Eng Part I-J Syst Control Eng, 2022, 236: 1630–1648
11 Cao X, Zhang C, Zhao D, et al. Event-triggered consensus control of continuous-time stochastic multi-agent systems. Automatica, 2022, 137: 110022
12 Mu C, Wang K, Sun C. Learning control supported by dynamic event communication applying to industrial systems. IEEE Trans Ind Inf, 2020, 17: 2325–2335
13 Liu G, Sun Q, Wang R, et al. Reduced-order observer-based fuzzy adaptive dynamic event-triggered consensus control for multi-agent systems with communication faults. Nonlinear Dyn, 2022, 110: 1421–1435
14 Sathishkumar M, Liu Y C. Resilient memory event-triggered consensus control for multi-agent systems with aperiodic DoS attacks. Int J Control Autom Syst, 2022, 20: 1800–1813
15 Cong M, Mu X, Hu Z. Sampled-data-based event-triggered secure bipartite tracking consensus of linear multi-agent systems under DoS attacks. J Franklin Institute, 2021, 358: 6798–6817
16 Yang Y, Li Y F, Yue D. Event-trigger-based consensus secure control of linear multi-agent systems under DoS attacks over multiple transmission channels. Sci China Inf Sci, 2020, 63: 150208
17 Zhang Y F, Wu Z-G, Wu Z Z, et al. Resilient observer-based event-triggered control for cyber-physical systems under asynchronous denial-of-service attacks. Sci China Inf Sci, 2022, 65: 142203
18 Guo X G, Liu P M, Wang J L, et al. Event-triggered adaptive fault-tolerant pinning control for cluster consensus of heterogeneous nonlinear multi-agent systems under aperiodic DoS attacks. IEEE Trans Netw Sci Eng, 2021, 8: 1941–1956
19 Deng C, Zhang D, Feng G. Resilient practical cooperative output regulation for MASs with unknown switching exosystem dynamics under DoS attacks. Automatica, 2022, 139: 110172
20 Ahmed Z, Khan M M, Saeed M A, et al. Consensus control of multi-agent systems with input and communication delay: a frequency domain perspective. ISA Trans, 2020, 101: 69–77
21 Hajshirmohamadi S, Sheikholeslam F, Meskin N. Distributed simultaneous fault detection and leader-following consensus control for multi-agent systems. ISA Trans, 2019, 87: 129–142
22 Huang X, Chen Y, Zhan J. Observer-based consensus control for multi-agent systems with measurement noises and external disturbances. Intl J Robust Nonlinear, 2022, 32: 344–357
23 Yu T, Ma L, Zhang H. Prescribed performance for bipartite tracking control of nonlinear multiagent systems with hysteresis input uncertainties. IEEE Trans Cybern, 2018, 49: 1327–1338
24 Wang W, Liang H, Pan Y, et al. Prescribed performance adaptive fuzzy containment control for nonlinear multiagent systems using disturbance observer. IEEE Trans Cybern, 2020, 50: 3879–3891
25 Wu Y, Yue D. Prescribed performance global stable adaptive neural dynamic surface consensus tracking control of stochastic multi-agent systems with hysteresis inputs and nonlinear dynamics. Int J Syst Sci, 2018, 49: 3431–3447
26 Xu Y, Fang M, Wu Z G, et al. Input-based event-triggering consensus of multiagent systems under denial-of-service attacks. IEEE Trans Syst Man Cybern Syst, 2020, 50: 1455–1464

27 Zhang D, Feng G. A new switched system approach to leader-follower consensus of heterogeneous linear multiagent systems with DoS attack. IEEE Trans Syst Man Cybern Syst, 2021, 51: 1258–1266
28 Sun Y C, Yang G H. Periodic event-triggered resilient control for cyber-physical systems under denial-of-service attacks. J Franklin Inst, 2018, 355: 5613–5631
29 Wu Z, Wu Y, Yue D. Distributed adaptive neural consensus tracking control of MIMO stochastic nonlinear multiagent systems with actuator failures and unknown dead zones. Adaptive Control Signal, 2018, 32: 1694–1714
30 Wu Y, Liang H, Zhang Y, et al. Cooperative adaptive dynamic surface control for a class of high-order stochastic nonlinear multiagent systems. IEEE Trans Cybern, 2020, 51: 5214–5224
31 Wang W, Wen C, Huang J. Distributed adaptive asymptotically consensus tracking control of nonlinear multi-agent systems with unknown parameters and uncertain disturbances. Automatica, 2017, 77: 133–142
32 Liu Z, Lai G, Zhang Y, et al. Adaptive fuzzy tracking control of nonlinear time-delay systems with dead-zone output mechanism based on a novel smooth model. IEEE Trans Fuzzy Syst, 2015, 23: 1998–2011
33 Liu Y J, Lu S, Tong S, et al. Adaptive control-based Barrier Lyapunov Functions for a class of stochastic nonlinear systems with full state constraints. Automatica, 2018, 87: 83–93
34 Li K, Hua C C, You X, et al. Distributed output-feedback consensus control of multiagent systems with unknown output measurement sensitivity. IEEE Trans Automat Contr, 2020, 66: 3303–3310
35 Zhao K, Song Y, Ma T, et al. Prescribed performance control of uncertain Euler-Lagrange systems subject to full-state constraints. IEEE Trans Neural Networks Learn Syst, 2017, 29: 3478–34893